Inorganic Chemistry

Article

pubs.acs.org/IC

# Fresh Look at the Mystery of Magnetization Reversal in $YVO_3$

Alexei A. Belik*

International Center for Materials Nanoarchitectonics (WPI-MANA), National Institute for Materials Science (NIMS), 1-1 Namiki, Tsukuba, Ibaraki 305-0044, Japan

Supporting Information

**ABSTRACT:** Phase transitions and detailed magnetic properties of polycrystalline AP-$YVO_{3.00(1)}$ (prepared at ambient pressure by a conventional solid-state method) and polycrystalline HP-$YVO_{3.04(1)}$ and HP-$YVO_{3.05(1)}$ (AP-$YVO_3$ treated at 6 GPa and 1600 K during 130 and 15 min, respectively) were investigated. The three samples showed a remarkable exchange bias (EB) effect. HP-$YVO_{3.04}$ and HP-$YVO_{3.05}$ had similar chemical composition, crystallographic parameters, and particle size, but their magnetic properties were qualitatively different. EB was negative at all temperatures in AP-$YVO_3$ and HP-$YVO_{3.05}$, resulting in the absence of magnetization reversal (MR). Positive EB was observed in HP-$YVO_{3.04}$ between $T_{N2}$ = 71 K and $T^*$ = 88 K resulting in MR or negative magnetization between those temperatures. It was demonstrated that polycrystalline HP-$YVO_{3.04}$ behaved similar to single crystals of $YVO_{3+\delta}$. By the careful control of the trapped magnetic field, measurement conditions were found under which no MR occurred in HP-$YVO_{3.04}$ at moderate magnetic fields, indicating that MR is not an intrinsic property of $YVO_{3+\delta}$. A drastic effect of trapped magnetic fields on MR and memory effects were observed. The importance of an "insignificant" anomaly at $T_{FM}$ = 140 K for MR was suggested. We also suggested that "positive exchange bias", "defects", "interfaces", and "pinning" should be keywords for understanding $YVO_3$ and probably other perovskite materials with the MR effect.

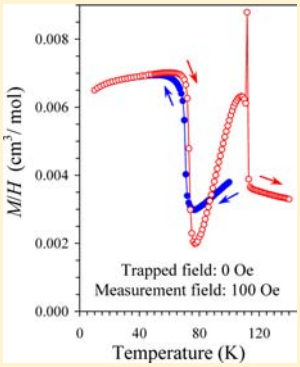


## 1. INTRODUCTION

Perovskite vanadates, $RVO_3$ ($R$ = Y and rare earths), have been attracting a lot of attention for decades.[1−16] One reason is rich phase diagrams and different spin and orbital ordering.[1,2] Another reason is the observation of the magnetization reversal (MR) or negative magnetization effect.[3−6] MR was originally predicted and observed in some ferrimagnets having several magnetic sublattices due to different temperature dependence of sublattice magnetizations. However, the origin of MR in $RVO_3$ and other perovskite-type compounds with one magnetic sublattice is still a matter of debate in the literature. Different explanations have been proposed.

MR was observed by Goodenough et al. in polycrystalline samples of $LaVO_3$ (below 138 K) but not in polycrystalline $YVO_3$ and $LuVO_3$.[3] This fact led to the idea that cooling through a first-order structural magnetostrictive transition in $LaVO_3$ could enhance the $V^{3+}$ orbital angular moment and reserve the Dzyaloshinsky vector to create a weak ferromagnetic component in a direction opposite to the applied field. Later, MR was observed in single crystals of $YVO_3$ (mainly along the $a$ axis (= 5.27722 Å) in the $Pbnm$ setting) below a second-order magnetic transition with $T_{N1}$ = 116 K.[5,6] This fact allowed proposing a different mechanism where the single-ion magnetic anisotropy and Dzyaloshinsky−Moriya interaction compete with each other and lead to negative magnetization. However, a fit based on this model resulted in the anisotropy term to be about 1.7 times the main exchange, and this result violated the assumptions of the model.[6] There were other problems with the model as discussed by Kimishima et al.[14,15] MR in polycrystalline $NdVO_3$ and $SmVO_3$ was explained based on the N-type ferrimagnetism model.[14,15] However, this model did not find experimental confirmations. It was suggested recently that MR in $RVO_3$ is caused by inhomogeneities from defects in the orbital sector of quasi-one-dimensional orbital systems.[16] A drastic effect of the trapped magnetic field inside a magnetometer was found on the MR process in $YVO_3$ in ref 16.

MR effects were observed in perovskite solid solutions. In polycrystalline $YFe_{0.5}Cr_{0.5}O_3$ and $BiFe_{0.5}Mn_{0.5}O_3$ with two different $B$-type cations, the competition between the single-ion magnetic anisotropy and different Dzyaloshinsky−Moriya interactions was also suggested as the origin.[17−20] However, two recent papers on $BiFe_{1-x}Mn_xO_3$ put forward sample inhomogeneities as the origin of MR.[21,22] MR was observed in perovskite solid solutions with two different $A$-type cations, e.g., polycrystalline $La_{0.15}Pr_{0.85}CrO_3$ and $La_{0.2}Ce_{0.8}CrO_3$.[23,24] In $La_{0.15}Pr_{0.85}CrO_3$, a $Pr^{3+}$-$Cr^{3+}$ coupling was assumed even though the ordering/effect of magnetic $A$-type cations occurs at low temperatures. The effect in $La_{0.2}Ce_{0.8}CrO_3$ nanoparticles was explained by their core−shell structure and the existence of a disordered shell with uncompensated spins, but spins from $Ce^{3+}$ were also assumed to have a contribution.[24]

It should be mentioned that the so-called exchange bias (EB) effect was detected in many cases when detailed magnetic studies have been performed on perovskite materials with MR.[17,21,23,24] The EB effect manifests itself in shifts of isothermal magnetization ($M$−$H$) curves relative to the origin depending on measurement conditions.[25] Shifts could occur in

Received: March 4, 2013
Published: July 22, 2013

   dx.doi.org/10.1021/ic401042x | Inorg. Chem. 2013, 52, 8529−8539

Table 1. Different Parameters of AP-$YVO_3$, HP-$YVO_3$, and HP-$YVO_3$(II)

| | sample | | |
|---|---|---|---|
| | AP-$YVO_3$ | HP-$YVO_3$(II) | HP-$YVO_3$ |
| synthesis | reduction of $YVO_4$ in 10% $H_2$ + 90% Ar at 1273 K for 4 h | treatment of AP-$YVO_3$ at 6 GPa and 1600 K for 15 min | treatment of AP-$YVO_3$ at 6 GPa and 1600 K for 130 min |
| oxygen content | $YVO_{2.998(10)}$ | $YVO_{3.053(10)}$ | $YVO_{3.041(10)}$ |
| lattice parameters[a] | | | |
| $a$ (Å) | 5.59715(10) | 5.60441(3) | 5.60429(4) |
| $b$ (Å) | 7.58268(14) | 7.57378(4) | 7.57220(5) |
| $c$ (Å) | 5.28261(10) | 5.27839(3) | 5.27761(4) |
| $V$ (Å$^3$) | 224.207(7) | 224.050(2) | 223.965(2) |
| $b/\sqrt{2}c$ | 1.0150 | 1.0146 | 1.0145 |
| experimental density (g/cm$^3$)[b] | 5.49(2) - powder | 5.535(10) - pellet | 5.540(10) - pellet; 5.53(2) - powder |
| particle size | Average: 63 nm | ~1−5 $\mu$m | ~5−15 $\mu$m |
| $T_{OO}$ from DSC (K) | 196 | 196 | 195 |
| $T_{N1}$ (K), from peaks on $\chi'$ vs $T$ | 117 | 113 | 112.4 |
| $T_{N1}$ (K)[c] | 118 | 114 | 114 |
| $T_{N2}$ (K)[c] | 80 | 78 | 71 |
| $T_{FM}$ (K)[c] | 145 | 135−140 | 140 |
| exchange bias | negative at all temperatures | negative at all temperatures | positive between 71 and 88 K |
| negative magnetization | No | No | yes, between 71 and 88 K |

[a]Single crystal data: $a$ = 5.60453(3) Å, $b$ = 7.57294(4) Å, $c$ = 5.27722(3) Å.[13] [b]The accuracy of density measurements was checked by measurements of commercial single crystals of $SrTiO_3$, $LaAlO_3$, and $YVO_4$, where the perfect agreement between calculated and experimental densities was found (see the Supporting Information). [c]From peaks on $dc$ FCC $d\chi/dT$ vs $T$ curves at 100 Oe.

the left direction relative to the origin (negative EB) or the right direction (positive EB). When negative and positive EB is observed on one sample depending on temperature or cooling conditions, it is called tunable EB. EB has been observed in core−shell nanoparticles, phase separated bulk materials, and in many multilayered thin films.[25] In other words, EB requires interfaces or inhomogeneities. The EB effect was observed in polycrystalline $YVO_3$,[3] $LuVO_3$,[3] $SmVO_3$,[14] and $NdVO_3$,[15] but left without proper explanation and attention. The (tunable) EB was found in polycrystalline $La_{0.15}Pr_{0.85}CrO_3$,[23] $La_{0.2}Ce_{0.8}CrO_3$,[24] $YFe_{0.5}Cr_{0.5}O_3$,[17] and $BiFe_{0.6}Mn_{0.4}O_3$.[21]

In this paragraph, we summarize additional information about $YVO_3$ because our work is focused on this compound. $YVO_3$ is typical Mott−Hubbard antiferromagnetic insulator with $V^{3+}$ ($S$ = 1, $S$ is spin) magnetic ions. Two antiferromagnetic phase transitions occur at $T_{N1}$ = 116 K (C-type spin ordering) and $T_{N2}$ = 77 K (G-type spin ordering), and two types of orbital ordering were observed below $T_{OO}$ = 200 K (G-type) and $T_{N2}$ (C-type). $YVO_3$ crystallizes in the $GdFeO_3$-type perovksite structure at room temperature (space group $Pnma$; lattice parameters $a$ = 5.60608 Å, $b$ = 7.57421 Å, and $c$ = 5.27839 Å;[12] $a$ = 5.60453 Å, $b$ = 7.57294 Å, and $c$ = 5.27722 Å).[13] There is a second-order structural phase transition at $T_{OO}$ to the monoclinic $P2_1/n$ space group, and a first-order structural phase transition at $T_{N2}$ back to the orthorhombic $Pnma$ space group. We emphasize that so far, magnetization reversal was found only in single crystals of $YVO_3$.[4−6,16] It was found that magnetization changes its sign below about $T^*$ = 95 K and then switches back below $T_{N2}$; changes of signs were always observed on crossing $T_{N2}$ and $T^*$ in modest magnetic fields independent of field-cooled (FC) or zero-field-cooled (ZFC) regimes.[5,6] The difference between ZFC and FC curves was observed below $T_{SO}$ = 130 K (we will call it $T_{FM}$) in polycrystalline $YVO_3$ in early papers on $YVO_3$,[3,26] but this anomaly remains without attention in further papers especially on single crystals. It was suggested that short-range order takes place at $T_{FM}$.[3,26] Some anomalies were found in Debye−Waller factors near 150 K; they were ascribed to the appearance of local structural disorder on V atoms.[27]

We believe that there should be a general mechanism of MR in different perovskite materials mentioned above because they demonstrate very similar magnetic behavior through their $T_N$s. Therefore, in this work, we reinvestigated a classical system, $YVO_3$, using detailed magnetic measurements. $YVO_3$ has one type and nonmagnetic $Y^{3+}$ ions. Therefore, the $A$-type sublattice should not play a role. There is one type of $B$ cations, and there is only one crystallographic site for $V^{3+}$ ions in the $Pnma$ structure. Therefore, many proposed mechanisms of MR in perovskite materials can be ruled out immediately. Some polycrystalline samples of $YVO_3$ were shown to behave similar to single crystals. A remarkable EB effect responsible for MR was observed. We proposed that fundamental questions for understanding $YVO_3$ and other perovskite materials should be "what are the origin and mechanism of EB in single-phase materials?" and "what are the origin and mechanism of tunable EB?"

## 2. EXPERIMENTAL SECTION

$YVO_4$ was first prepared from a stoichiometric mixture of $Y_2O_3$ and $V_2O_5$ by heating at 923 K for 30 h followed by annealing at 1273 K for 70 h in an $Al_2O_3$ crucible with several intermediate grindings. Single-phase $YVO_4$ was then reduced in a mixture of 10% $H_2$ and 90% Ar at 1273 K for 4 h. The resultant sample was a single-phase $YVO_3$ powder. Its oxygen content was determined to be $YVO_{2.998(10)}$ from the thermogravimetric (TG) analysis in air (from the weight gain corresponding to oxidation of $YVO_{3+\delta}$ to $YVO_4$; see the Supporting Information). This sample will be called AP-$YVO_3$, where AP stands for ambient-pressure. AP-$YVO_3$ was treated at 6 GPa in a belt-type high pressure apparatus at 1600 K for 130 and 15 min with the heating rate of 130 K/min. After heat treatment, the samples were quenched to room temperature (RT), and the pressure was slowly released. The resultant samples were dense pellets (Table 1) and will be called HP-$YVO_3$ (for the sample annealed for 130 min) and HP-$YVO_3$(II) (for


dx.doi.org/10.1021/ic401042x | Inorg. Chem. 2013, 52, 8529−8539

the sample annealed for 15 min), where HP stands for high-pressure. The oxygen content was HP-$YVO_{3.041(10)}$ and HP-$YVO_{3.053(10)}$(II) (see Table 1). For simplicity, the $YVO_3$ formulas will be used in most parts of the paper.

X-ray powder diffraction (XRPD) data were collected at RT on a RIGAKU Ultima III diffractometer using Cu$K_\alpha$ radiation ($2\theta$ range from 19° to 140 (150)°, a step width of 0.02°, and a counting time of 10 s/step). The XRPD data were analyzed by the Rietveld method with RIETAN-2000.[28] Density was measured using the Archimedes method using $CCl_4$ with the density of 1.5867 g/cm$^3$.

For the TG analysis, experiments were performed in a usual furnace in air (heating rate 5 K/min, annealed at 1173 K for 1 h) in Pt holders, and we weighted powdered samples before and after the oxidation. All samples were dried at 413 K for 24 h before the TG experiments. One TG/DTA experiment was performed in air on a SII Exstar 6000 (TG-DTA 6200) system between 300 and 1173 K at a heating−cooling rate of 5 K/min in a Pt holder. Differential scanning calorimetry (DSC) curves were recorded using powdered samples on a Mettler Toledo DSC1 STAR$^e$ system at a heating/cooling rate of 5 K/min under $N_2$ flow between 293 and 148 K in Al capsules. Several DSC runs were performed to check the reproducibility, and good reproducibility was observed.

Temperature-dependent magnetization measurements were performed on a SQUID magnetometer (Quantum Design, MPMS 1T) between 2 and 10 and 300−350 K in different applied fields under both zero-field-cooled (ZFC) conditions on warming and field-cooled (FC) conditions on cooling (FCC) and warming (FCW) in the "settle" mode. In the FCC regime, a sample was usually measured on cooling from the maximum measurement temperature after a ZFC measurement. In the FCW regime, a sample was inserted into a magnetometer at 300 K, then a magnetic field was applied, and then temperature was set to the lowest temperature with the rate of 10 K/min; a measurement was performed on warming. In the ZFC regime, two cooling procedures were used. In the first procedure (which is a standard and typically used procedure in our laboratory), a sample was rapidly (within 3−5 min) inserted into a magnetometer, which was kept at 10 K. This procedure will be called q-ZFC, where q stands for quenched. In the second procedure, a sample was inserted into a magnetometer kept at 300 K, then temperature was set to 5−10 K with the rate of 10 K/min, and at 5−10 K, a magnetic field was applied. This procedure will be called s-ZFC, where s stands for slow (cooled).

We paid special attention on a trapped field (TF) inside magnetometers for q-ZFC and s-ZFC measurements and measurements in low magnetic fields. Our Quantum Design MPMS instrument has the "reset magnet" option, where a superconducting magnet is warmed. The "reset magnet" option reduces the absolute value of the trapped magnetic field below about 0.01 Oe (but the sign of the field was negative in most cases, e.g., $M$(Nb) ≈ +5.0 × 10$^{-6}$ emu at 5 K). Then, we used an Nb superconducting sample and the iterative process to set (if needed) the trapped magnetic field to a positive value; however, with the process the TF could be reduced below 0.1 Oe at the sample position (that is, we reduced the absolute value of the magnetization ($M$) of a powder Nb sample (about 100 mg) below 10$^{-4}$ emu at 5 K, cf., $M$(Nb) = −1.22 × 10$^{-3}$ emu at 1 Oe, $M$(Nb) = −1.32 × 10$^{-2}$ emu at 10 Oe, $M$(Nb) = −6.52 × 10$^{-2}$ emu at 50 Oe, and $M$(Nb) = −1.30 × 10$^{-1}$ emu at 100 Oe). Therefore, a positive trapped magnetic field below 0.1 Oe will be called the "zero field" throughout the paper, and all ZFC measurements were performed under this condition. In some cases, we intentionally set a positive trapped field (PTF) or a negative trapped field (NTF) of about 1−2 Oe after the "reset magnet" procedure as specified in each case below. The sign of the trapped magnetic field was checked by the Nb sample. However, we did not adjust the real value of the trapped field to the nominal value.

Isothermal magnetization measurements were performed in the "settle" and "no overshoot" mode between −10 to 10 kOe on MPMS 1T and between −50 to 50 kOe on MPMS 5T at different temperatures using the ZFC and FC regimes. In the FC regime, a sample was cooled to a desired temperature at 10 kOe (50 kOe, or 100 Oe) from 300 K with the cooling rate of 10 K/min. Details are specified in the text for each measurement.

Frequency dependent *ac* susceptibility measurements at a zero static magnetic field were performed with a Quantum Design PPMS instrument from 300 to 5 K at frequencies ($f$) of 0.5, 1, 5, and 10 kHz and an applied oscillating magnetic field ($H_{ac}$) of 10 Oe and on a Quantum Design MPMS instrument from 300 to 2 K at $f$ = 300 kHz and $H_{ac}$ = 5 Oe. Specific heat, $C_p$, at 0 Oe and 90 kOe was recorded for HP-$YVO_3$ and HP-$YVO_3$(II) between 2 and 300 K on cooling and heating by a pulse relaxation method using a commercial calorimeter (Quantum Design PPMS). No noticeable difference was found between curves at 0 Oe and 90 kOe (see Figure S21 in the Supporting Information).

A powder AP-$YVO_3$ sample and dense pellets of HP-$YVO_3$ and HP-$YVO_3$(II) were used in all magnetic measurements (except for Figures S23−S25 in the Supporting Information). We emphasize that we checked two different orientations of a piece of a pellet of HP-$YVO_3$ in respect to a magnetic field and checked different parts of a pellet; FCC curves at 100 Oe and $M$−$H$ curves were identical. This fact showed that pellets had no preferred orientation. We used pellets to prevent particle movements during measurements. The powder AP-$YVO_3$ sample was tightly wrapped by plastic tape or mixed with an Apiezon N-grease to prevent particle movements. We found no principal difference between two types of fixation.

## 3. RESULTS

**3.1. Structural Properties.** Figures 1 and 2 show the XRPD patterns of AP-$YVO_3$, HP-$YVO_3$, and HP-$YVO_3$(II). All samples were single-phase. The refined lattice parameters are given in Table 1. The refined structural parameters are reported in Table S1 in the Supporting Information. All the parameters were in very good agreement with the reported values. Figure 2, which shows the XRPD patterns in the $2\theta$ range of 100−140°, illustrates that HP-$YVO_3$ and HP-$YVO_3$(II) were almost identical. The average particle size of AP-$YVO_3$ estimated with the Scherrer equation was about 63 nm. The grain size of HP-$YVO_3$ estimated with an optical microscope was between about 5 and 15 $\mu$m, and that of HP-$YVO_3$(II) was between about 1 and 5 $\mu$m (see Figure S2 in the Supporting Information).

**3.2. DSC Studies Across $T_{OO}$.** DSC curves of AP-$YVO_3$, HP-$YVO_3$, and HP-$YVO_3$(II) across $T_{OO}$ are shown in Figure 3. DSC anomalies in AP-$YVO_3$ were noticeably smeared in comparison with HP-$YVO_3$ and HP-$YVO_3$(II): the DSC anomaly (on heating) ended at about 211 K in AP-$YVO_3$, but at about 202−203 K in HP-$YVO_3$ and HP-$YVO_3$(II). Smearing could be caused by nanosized particles of AP-$YVO_3$. Both HP-$YVO_3$ and HP-$YVO_3$(II) demonstrated almost identical anomalies at $T_{OO}$. The $T_{OO}$ values were determined from peak positions on the DSC heating curves, and they are given in Table 1.

**3.3. Specific Heat Studies of HP-$YVO_3$ and HP-$YVO_3$(II).** Figure 4 depicts the $C_p/T$ vs $T$ and $C_p$ vs $T$ curves of HP-$YVO_3$ and HP-$YVO_3$(II). (Specific heat of AP-$YVO_3$ was not measured because only powder was available). There were anomalies at $T_{OO}$, $T_{N1}$, and $T_{N2}$ in HP-$YVO_3$. There was a drop in the $C_p/T$ values at $T_{N2}$ on cooling and a clear anomaly on heating in HP-$YVO_3$. These features are artifacts of the pulse relaxation method. This method sometimes cannot give reliable values of $C_p$ for first-order phase transitions. The drop of the $C_p/T$ values at $T_{N2}$ was often observed in previous papers (sometimes because of the detachment of a sample from a holder).[12,16] Specific heat anomalies were noticeable smeared in HP-$YVO_3$(II) at $T_{OO}$ (in comparison with the DSC curves) and


dx.doi.org/10.1021/ic401042x | Inorg. Chem. 2013, 52, 8529−8539

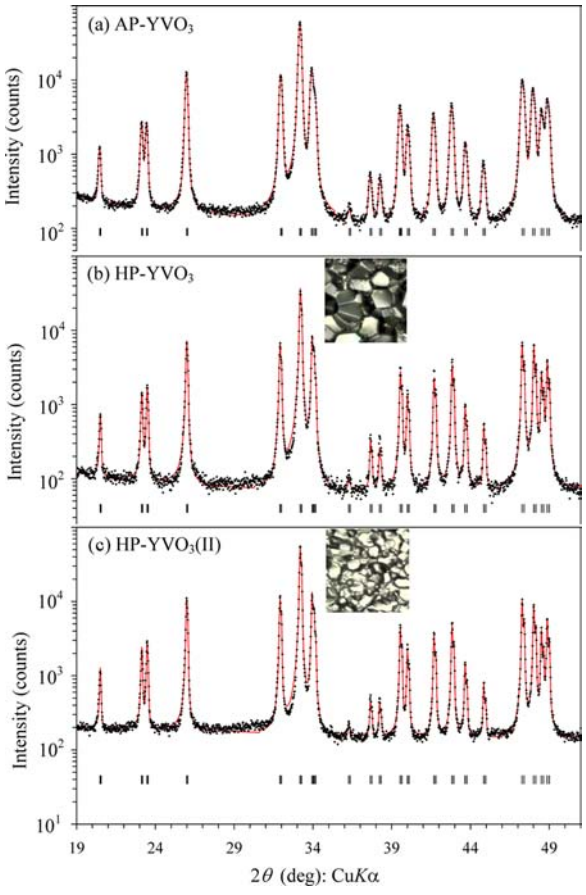


**Figure 1.** Fragments of experimental (black crosses) and calculated (red line) XRPD patterns of (a) AP-$YVO_3$, (b) HP-$YVO_3$, and (c) HP-$YVO_3$(II) between $2\theta$ = 19−50° in the logarithmic scale. The bars show possible Bragg reflection positions. The inserts show optical microscope images of pellets of HP-$YVO_3$ and HP-$YVO_3$(II); the side of the square is 20 $\mu$m.

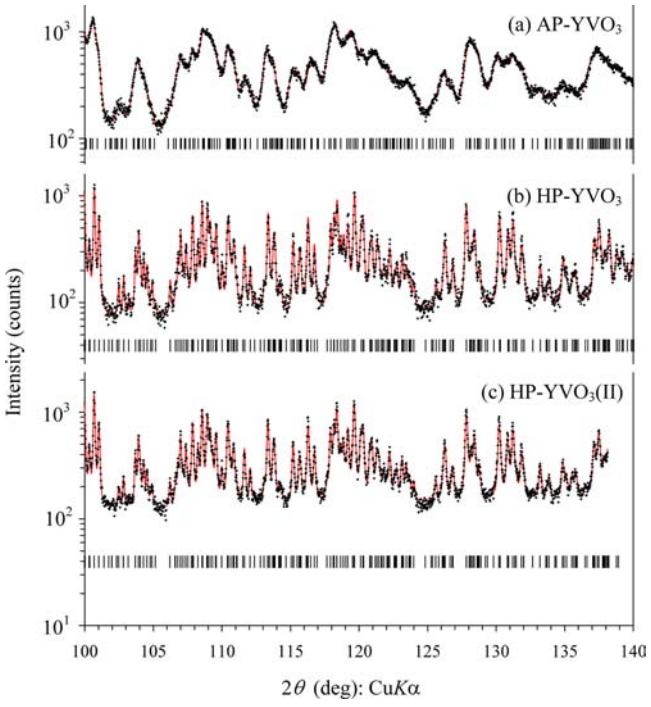


**Figure 2.** Fragments of experimental (black crosses) and calculated (red line) XRPD patterns of (a) AP-$YVO_3$, (b) HP-$YVO_3$, and (c) HP-$YVO_3$(II) between $2\theta$ = 100−140° in the logarithmic scale. The bars show possible Bragg reflection positions.

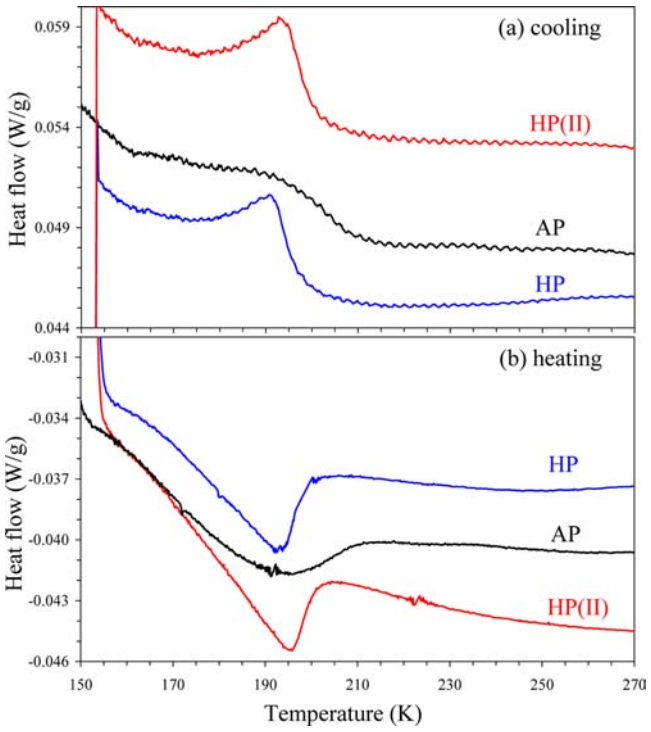


**Figure 3.** Differential scanning calorimetry curves of AP-$YVO_3$, HP-$YVO_3$, and HP-$YVO_3$(II) on (a) cooling and (b) heating (5 K/min) showing anomalies near $T_{OO}$. The second runs are shown.

$T_{N1}$, and no anomalies were observed at $T_{N2}$ on both cooling and heating.

**3.4. *ac* Susceptibility Studies.** $\chi'$ vs $T$ and $\chi''$ vs $T$ curves of the three samples are given in Figure 5. Both $\chi'$ vs $T$ and $\chi''$ vs $T$ curves showed sharp peaks at $T_{N1}$ (the peaks were centered at 112.4 K) in HP-$YVO_3$ indicating the appearance of a weak ferromagnetic state (due to spin canting). No $\chi''$ vs $T$ anomalies were detected at $T_{N2}$ and the $\chi'$ values dropped at $T_{N2}$ indicating that there should be no weak ferromagnetic moments or at least no significant changes in weak ferromagnetic moments below $T_{N2}$ in comparison with the $T_{N2} < T < T_{N1}$ interval in HP-$YVO_3$.

$\chi'$ vs $T$ and $\chi''$ vs $T$ curves were noticeable different in AP-$YVO_3$ and HP-$YVO_3$(II). Almost no anomalies were observed at $T_{N1}$ (and no anomalies at $T_{N2}$) on the $\chi''$ vs $T$ curves. No noticeable anomalies were observed at $T_{N2}$ on the $\chi'$ vs $T$ curves. The peak at $T_{N1}$ (observed at 117 K in AP-$YVO_3$ and 113 K in HP-$YVO_3$(II)) on the $\chi'$ vs $T$ curves was noticeably weaker and broader than the peak in HP-$YVO_3$.

We emphasize that a kink was observed at $T_{OO}$ and no anomalies were observed at $T_{FM}$ (~140 K) on the *ac* susceptibility curves of the three samples.

**3.5. *dc* Magnetic Studies.** *3.5.1. AP-$YVO_3$.* *dc* magnetic susceptibilities of AP-$YVO_3$ are shown in Figure 6. No MR was observed on ZFC curves when TF was zero or positive. With NTF, negative magnetization was detected on ZFC curves (see Figure S4 in the Supporting Information), but this is a usually observed artifact for materials having a (weak) ferromagnetic moment.[29] (When the coercive field and remnant magnet-


dx.doi.org/10.1021/ic401042x | Inorg. Chem. 2013, 52, 8529−8539

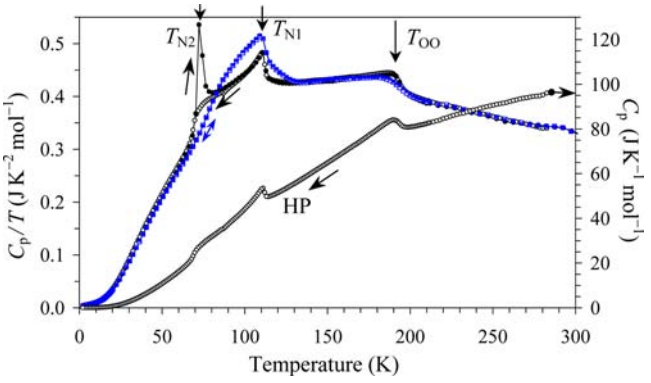


**Figure 4.** Specific heat data of HP-$YVO_3$ (circles) and HP-$YVO_3$(II) (squares) at a zero magnetic field on cooling (white circles and squares) and heating (filled circles and squares) plotted as $C_p/T$ vs $T$ (the left-hand axis) and $C_p$ vs $T$ (the right-hand axis). Vertical arrows show phase transitions. Measurements were performed at least twice to confirm reproducibility (see the Supporting Information).

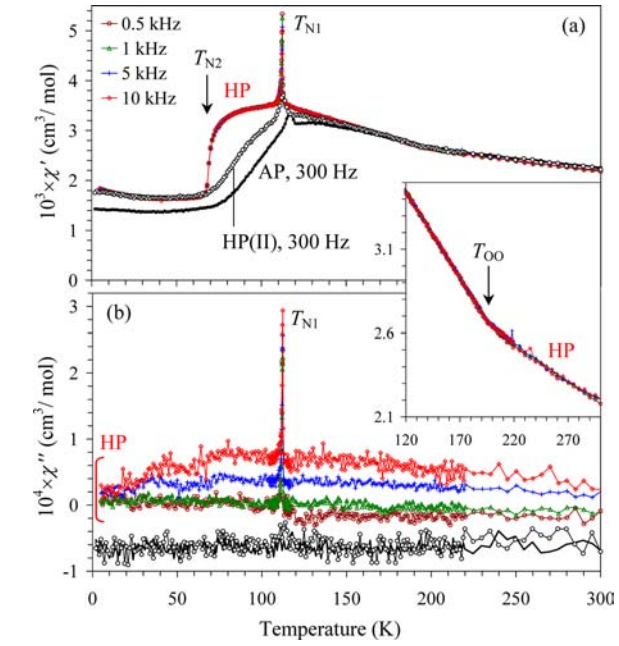


**Figure 5.** (a) Real $\chi'$ and (b) imaginary $\chi''$ parts of the *ac* susceptibilities as a function of temperature (2−300 K) of AP-$YVO_3$, HP-$YVO_3$, and HP-$YVO_3$(II). Measurements were performed on cooling at a zero static field using the *ac* field with the amplitude $H_{ac}$ = 10 Oe (HP-$YVO_3$) and $H_{ac}$ = 5 Oe (AP-$YVO_3$ and HP-$YVO_3$(II)) at different frequencies. The $\chi''$ vs $T$ curves of AP-$YVO_3$ and HP-$YVO_3$(II) were shifted for the clarity. The insert shows a kink at $T_{OO}$ in HP-$YVO_3$ on the $\chi'$ vs $T$ curve.

ization are small near $T_N$ or $T_C$, even a small negative magnetic field can form a domain structure with a preferential magnetization direction (instead of random field directions). At low temperatures, when the coercive field and remnant magnetization are much larger, a moderate positive field cannot reverse those domains resulting in negative magnetization). No MR was also observed on FCC (Figure 7a) and FCW (Figure S5, Supporting Information) measurements. The difference between the ZFC and FCC curves and the field dependence of the FCC curves was observed below $T_{FM}$ (about 145 K). These results are in agreement with all previous reports on magnetic properties of polycrystalline AP-$YVO_3$.[3,26] We observed a kink

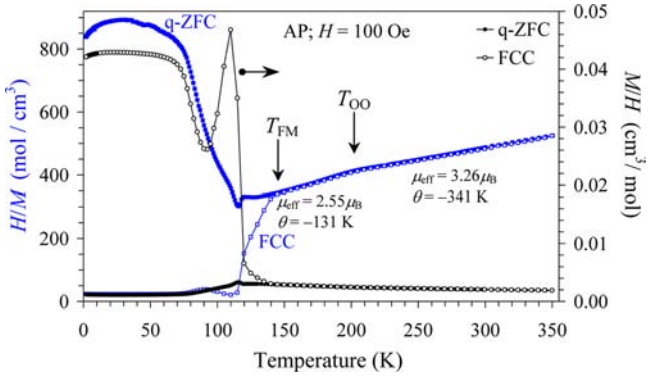


**Figure 6.** q-ZFC (filled symbols) and FCC (white symbols) *dc* magnetic susceptibility ($\chi = M/H$) curves of AP-$YVO_3$ at 100 Oe (the right-hand axis). The left-hand axis gives the same inverse curves ($H/M$ vs $T$). The parameters ($\mu_{eff}$ and $\theta$) of the Curie−Weiss fits below and above $T_{OO}$ are given.

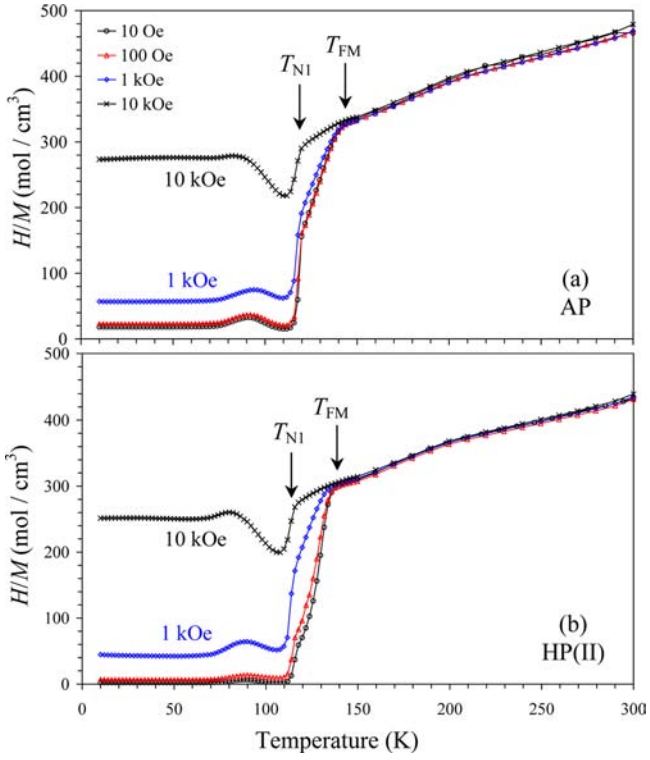


**Figure 7.** FCC $H/M$ vs $T$ curves of (a) AP-$YVO_3$ and (b) HP-$YVO_3$(II) at 10, 100, 1000, and 10000 Oe. Only FCC curves were recorded (without ZFC curves).

at $T_{OO}$ similar to single crystals,[6] and this feature has not been reported before, to the best of our knowledge, for polycrystalline AP-$YVO_3$.

In our work, we determined/defined magnetic transition temperatures from peak (anomaly) positions on the FCC $d\chi/dT$ vs $T$ curves at 100 Oe (see Table 1 and Figure S5 in the Supporting Information). The $d\chi/dT$ vs $T$ anomaly near $T_{N2}$ was rather broad and weak, but this is the only way to define $T_{N2}$ because only *dc* magnetic measurements showed some anomalies.

*3.5.2. HP-$YVO_3$(II).* All *dc* magnetic susceptibilities of HP-$YVO_3$(II) were qualitatively similar with those of AP-$YVO_3$ (Figure 7b and Figures S26, S28, and S29, Supporting Information), but with some quantitative differences (Figure


dx.doi.org/10.1021/ic401042x | Inorg. Chem. 2013, 52, 8529−8539

S30, Supporting Information). Importantly, no MR was observed on *dc* magnetic susceptibilities of HP-$YVO_3$(II). The phase transition temperatures are summarized in Table 1.

*3.5.3. FC Curves of HP-$YVO_3$.* *dc* magnetic susceptibilities of HP-$YVO_3$ were qualitatively different (Figure 8). FCC curves

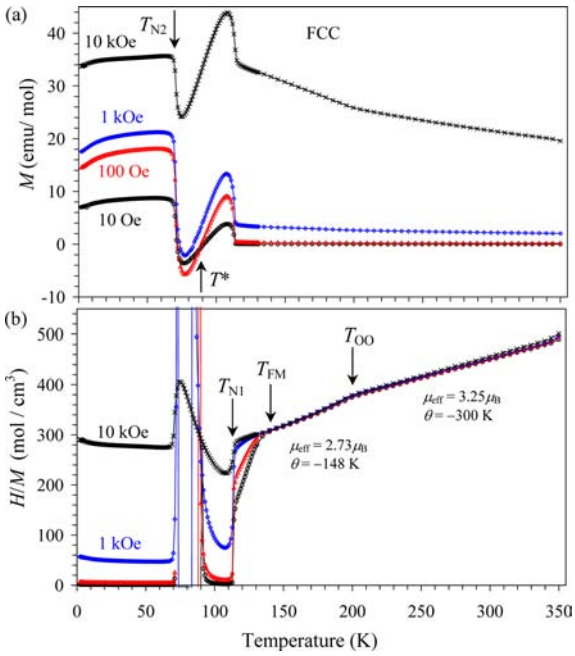


**Figure 8.** (a) FCC magnetization curves ($M$ vs $T$) of HP-$YVO_3$ at 10, 100, 1000, and 10000 Oe. (b) Same curves plotted as $H/M$ vs $T$. The parameters ($\mu_{eff}$ and $\theta$) of the Curie–Weiss fits below and above $T_{OO}$ are given. The vertical arrows show magnetic anomalies and characteristic temperatures. Only FCC curves were recorded (without ZFC curves).

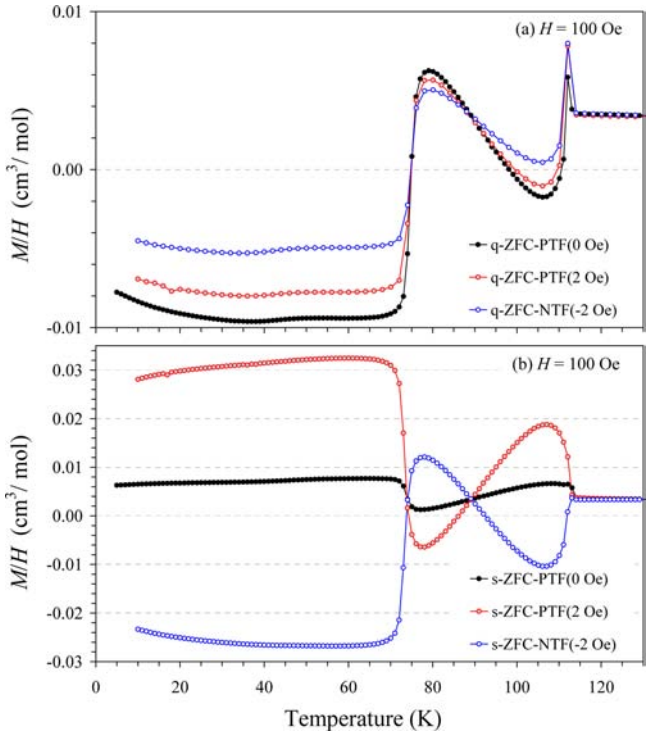


**Figure 9.** (a) q-ZFC susceptibility curves ($M/H$ vs $T$) of HP-$YVO_3$ measured at 100 Oe. The sample was rapidly (within 3–5 min) inserted into a magnetometer (which was kept at 10 K) having different trapped magnetic fields (PTF: a positive trapped field, NTF: a negative trapped field). (b) s-ZFC susceptibility curves ($M/H$ vs $T$) of HP-$YVO_3$ measured at 100 Oe. The sample was inserted into a magnetometer at 300 K and having different trapped fields, then temperature was set to 5–10 K at the rate of 10 K/min, and then a magnetic field of 100 Oe was applied.

resembled those of single crystals of $YVO_3$ (see also Figures S8–S12 in the Supporting Information,).[6,16] A classical form of the FCC and FCW curves with MR effects was observed at 10, 100, and 1000 Oe. Clear anomalies were observed at $T_{OO}$ = 200 K, $T_{FM}$ = 140 K, $T_{N1}$ =114 K, and $T_{N2}$ = 71 K on the $d\chi/dT$ vs $T$ curves (Figures S9 and S12, Supporting Information). As we mentioned, we defined transition temperatures from peak positions on the $d\chi/dT$ vs $T$ curves. Different definitions could be at the origin of slightly different values in comparison with the literature data (especially for $T_{N2}$ where a first-order transition takes place). MR took place at $T^*$ (about 88 K in our case) at 10 and 100 Oe. Above $T_{FM}$, there was no field dependence of magnetic susceptibilities indicating the absence of magnetic impurities with higher transition temperatures. Below $T_{FM}$, noticeable field dependence was observed (Figure 8b). This is a clear feature of the development of a weak ferromagnetic moment; this is why we call this temperature $T_{FM}$. The anomaly is observed only on the *dc* measurements. No anomalies could be seen on specific heat and *ac* susceptibilities.

*3.5.4. ZFC Curves of HP-$YVO_3$.* We performed detailed studies of ZFC curves of HP-$YVO_3$ (Figure 9). Independent of the value and sign of TF, q-ZFC curves had negative magnetization from 10 K to about $T_{N2}$, then positive from $T_{N2}$ to $T^*$, then negative or positive from $T^*$ to about $T_{N1}$, and finally positive again above about $T_{N1}$. The value and sign of TF had a more drastic effect on s-ZFC curves. The s-ZFC-NTF(−2 Oe) and s-ZFC-PTF(2 Oe) curves were almost symmetrical in respect to the line with $\chi$ = 0.0035 cm$^3$/mol (the value of susceptibility in a paramagnetic region just above $T_{N1}$) similar to single crystal data.[16] No (!) MR was detected when TF was kept as low as possible (during the s-ZFC-PTF(0 Oe) measurements). Finding just one condition under which no MR takes place proves that all other similar measurements (deferred by the value and sign of TF and the sample insertion procedure) are artifacts, and MR observed during those measurements is not intrinsic.

All the q-ZFC curves behaved similar to the s-ZFC-NTF(−2 Oe) curve. This result could be explained by nonuniform distribution of a magnetic field inside a magnet. The rapid movement of a sample through a magnet at low temperatures could cause preferential formation of domain structures with negative magnetization.

We also performed the following ZFC procedure: the HP-$YVO_3$ sample was cooled down from 300 K to a desired temperature between 10 and 110 K (below $T_{N1}$) in a zero magnetic field, then a magnetic field of 100 Oe was applied, and measurements were performed as a function of time up to 100 min (relaxation measurements (see Figure S13 in the Supporting Information)). The magnetization remained positive at all temperatures during this ZFC protocol, and the temperature dependence of susceptibilities followed the *ac* susceptibility curve instead of the *dc* susceptibility curve (Figure 10a; red circles), that is, there was a step-like decrease of susceptibilities at $T_{N2}$ instead of a step-like increase.


dx.doi.org/10.1021/ic401042x | *Inorg. Chem.* 2013, 52, 8529–8539

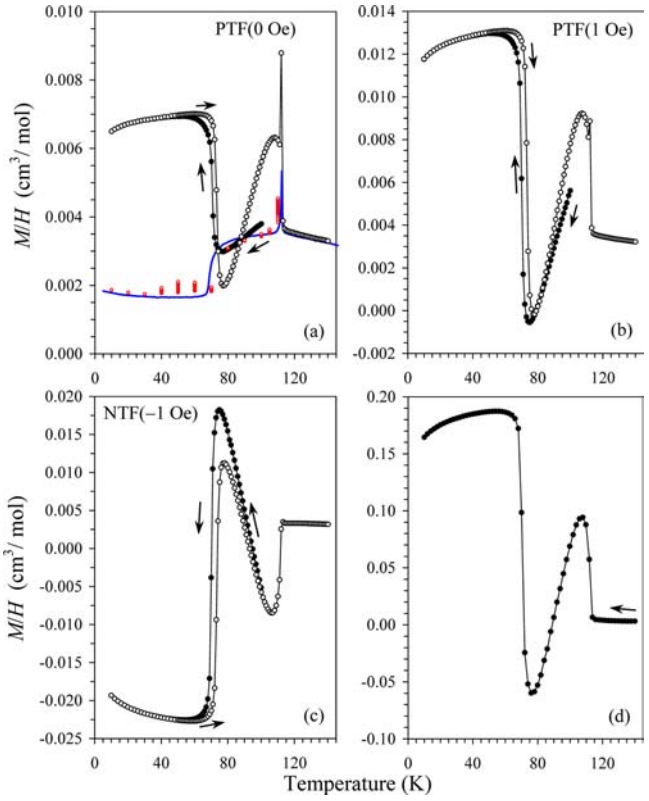


**Figure 10.** $M/H$ vs $T$ curves of HP-$YVO_3$. The sample was cooled down from 300 to 100 K at the rate of 10 K/min under different trapped fields: (a) 0 Oe, (b) 1 Oe, and (c) −1 Oe; then a magnetic field of 100 Oe was applied at 100 K, and the measurements were performed on cooling from 100 to 10 K (black circles; the first curve) and from 10 to 140 K (white circles; the second curve). (d) The third curve was measured from 140 to 10 K (at 100 Oe). The curve was identical for all three protocols (a), (b), and (c). In the panel (a), the $\chi'$ vs $T$ curve (from Figure 5a) is shown for comparison by the blue line; red circles show relaxation curves: the sample was cooled down from 300 K to a desired temperature in a zero magnetic field, then a magnetic field of 100 Oe was applied, and measurements were performed as a function of time up to 100 min (see Figure S13 in Supporting Information).

*3.5.5. Modified FC Curves of HP-$YVO_3$.* All FCC and FCW curves (at moderate fields, Figure 8 and Figures S9 and S10, Supporting Information) showed the MR effect. In standard measurement protocols, the sample was always cooled in a magnetic field from 300 K, that is, through $T_{N1}$. Considering the observation of (tunable) EB (see part 3.6), which requires cooling through $T_N$ of an antiferromagnet in a magnetic field, we modified the FC protocols as follows. The HP-$YVO_3$ sample was cooled down from 300 to 100 K (below $T_{N1}$) in a zero magnetic field or trapped magnetic fields of −1 and 1 Oe. At 100 K, a magnetic field of 100 Oe was applied, and measurements were performed from 100 to 10 K (the first curve), then from 10 to 140 K (the second curve), and finally from 140 to 10 K (the third curve). The results are presented in Figure 10. The third curve from 140 to 10 K was identical for all three runs (with PTF(0 Oe), PTF(1 Oe), and NTF(−1 Oe)) (Figure 10d). No (!) MR was detected when TF was zero even when the sample was cooled and warmed through $T_{N2}$ and $T^*$ at 100 Oe (Figure 10a) in contrast with the observations for single crystals.[6] With PTF of 1 Oe, a tiny MR took place near 75 K (Figure 10b). With NTF of −1 Oe, the initial magnetization was negative, then it changed to positive, and finally to negative again below $T_{N2}$ (Figure 10c). These results clearly showed that magnetic behavior depended on how the sample was cooled through $T_{N1}$. In other words, the sample remembered how it was cooled through $T_{N1}$: the sign of magnetization (below $T_{N2}$) reflected the sign of a (moderate) field during cooling through $T_{N1}$, and the value of magnetization (below $T_{N2}$) reflected the value of a (moderate) field during cooling through $T_{N1}$.

We emphasize again that finding just one condition under which no MR takes place proves that all other similar measurements (deferred by the value and sign of TF) are artifacts, and MR observed during those measurements is not intrinsic.

**3.6. Isothermal Magnetization Curves.** $M-H$ curves of AP-$YVO_3$, HP-$YVO_3$(II), and HP-$YVO_3$ are shown in Figure 11 and on Figures S16−S20, S27 in the Supporting Information. $M-H$ curves of HP-$YVO_3$(II) were qualitatively similar with those of AP-$YVO_3$ (the Supporting Information). The $M-H$ curves were basically linear between −10 kOe and 10 kOe without hysteresis below about 80 K. A tiny needle-like hysteresis opened between −50 kOe and 50 kOe (below 80 K; the Supporting Information) or above 80 K (Figure 11c). The FC measurements clearly demonstrated features of the EB effect: the $M-H$ curves exhibited almost parallel shifts. AP-$YVO_3$ always showed "up" shifts or negative EB (Figure 11d). HP-$YVO_3$ had "down" shifts or positive EB between $T_{N2}$ and $T^*$ (Figure 11b), and negative EB at other temperatures. The magnitude of the shift was the same for cooling in fields of 100 Oe and 10 kOe in HP-$YVO_3$ at 80 K (Figure S18d in the Supporting Information); this is a feature typically observed in multilayered thin films with EB.[25]

## 4. DISCUSSION

The structural parameters (fractional coordinates and V−O and Y−O bond lengths) of the three samples were very close to each other and to the reported parameters (see the Supporting Information). Therefore, the high-pressure synthesis does not modify the crystal structure of $YVO_3$.

The oxygen content of AP-$YVO_{2.998(10)}$ and HP-$YVO_{3.053(10)}$(II) was slightly different, and either were the lattice parameters and the DSC anomalies at $T_{OO}$. The particle size of AP-$YVO_3$ and HP-$YVO_3$(II) was quite different. Nevertheless, magnetic properties of AP-$YVO_3$ and HP-$YVO_3$(II) were surprisingly similar to each other. Both samples show qualitative similar $\chi'$ vs $T$ and $\chi''$ vs $T$ curves (but with slightly different transition temperatures), the absence of MR (particularly on FCC curves), and negative EB at all temperatures.

On the other hand, the oxygen content of HP-$YVO_{3.041(10)}$ and HP-$YVO_{3.053(10)}$(II) was the same within standard deviations and close the oxygen content of single crystals (the reported values were $YVO_{3.03(2)}$ and $YVO_{3.02}$).[6,12] The lattice parameters of HP-$YVO_3$ and HP-$YVO_3$(II) were very close to each other and to the lattice parameters of single crystals (Table 1). Because of the similar lattice parameters, the XRPD patterns in the $2\theta$ range of 100−140° were almost identical (Figure 2). Both facts, very similar chemical composition and lattice parameters, supplement each other. If the chemical composition of HP-$YVO_3$ and HP-$YVO_3$(II) were different, it would be reflected in the lattice parameters and XRPD patterns in the $2\theta$ range of 100−140°. The particle size of HP-$YVO_3$ and HP-$YVO_3$(II) was also of the same order of


dx.doi.org/10.1021/ic401042x | Inorg. Chem. 2013, 52, 8529−8539

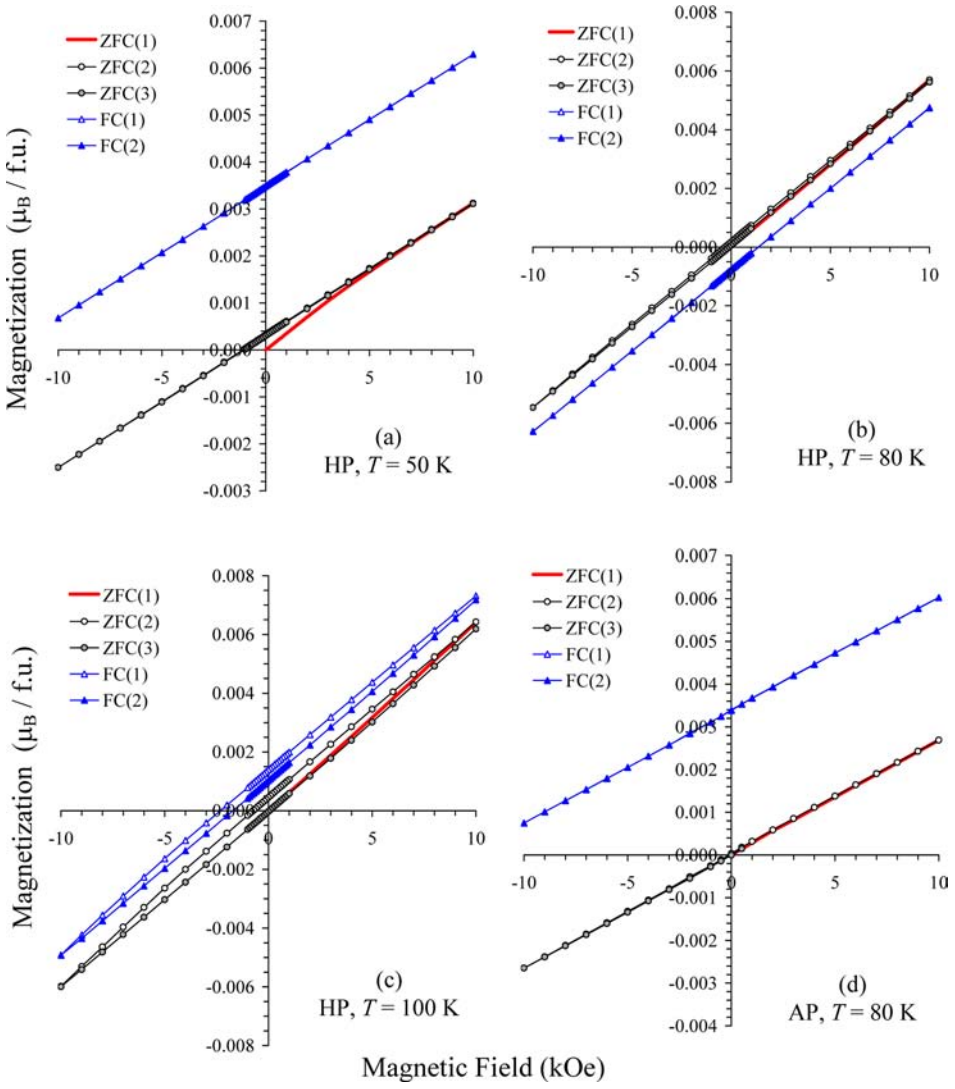


**Figure 11.** $M$ vs $H$ curves of HP-$YVO_3$ at (a) 50 K, (b) 80 K, and (c) 100 K and (d) AP-$YVO_3$ at 80 K under the ZFC and FC protocols. ZFC(1): the first brunch measured from 0 to 10 kOe; ZFC(2): the second brunch measured from 10 kOe to −10 kOe; ZFC (3): the third brunch measured from −10 kOe to 10 kOe. FC (1): the first brunch measured from 10 kOe to −10 kOe; FC (2): the second brunch measured from −10 kOe to 10 kOe.

magnitude (several micrometers), and the DSC anomalies at $T_{OO}$ were identical.

Despite the above similarities, magnetic properties of HP-$YVO_3$ and HP-$YVO_3$(II) were qualitatively different. HP-$YVO_3$ behaved similar to single crystals,[6,16] that is, it showed MR at $T^*$ and $T_{N2}$ when it was cooled through $T_{N1}$ at moderate magnetic fields (and even small trapped magnetic fields). HP-$YVO_3$ demonstrated also positive EB between $T^*$ and $T_{N2}$ (in the FC mode) in comparison with HP-$YVO_3$(II). Considering the above similarities, we can conclude that the average oxygen content is not a determinative factor of different magnetic properties. We note that the composition of AP phases without MR was reported to be $YVO_{3.03(1)}$[26] and $YVO_{3.00(2)}$[3] confirming again that the oxygen content itself does not determine magnetic properties. MR properties were strongly sample-dependent for almost identical samples, HP-$YVO_3$, HP-$YVO_3$(II), and another sample HP-$YVO_3$(b) (see Tables S1 and S3 and Figures S31−S34 in Supporting Information). This is an indication of an extrinsic origin of MR in oxygen nonstoichiometric HP-$YVO_{3.041}$. Intrinsic properties of $YVO_3$ seem to be represented by properties of the most stoichiometric AP-$YVO_3$.

The oxygen excess in perovskites ($ABO_{3+\delta}$) is usually understood as cation deficiency ($A_{1-x}B_{1-x}O_3$). Therefore, the HP-$YVO_{3.041}$ composition corresponds to HP-$Y_{0.987}V_{0.987}O_3$, which means the presence of a small amount of $V^{4+}$ ions at the $B$ site in addition to vacancies. The experimental density of HP-$YVO_3$ (Table 1) was slightly smaller than the calculated XRD density (about 5.57 g/cm$^3$) confirming a cation-deficient picture. The experimental density of AP-$YVO_3$ (Table 1) was even smaller and corresponded to a composition of $Y_{0.987}V_{0.987}O_{2.961}$. We note that crystal-structure analysis methods and analytical methods are not capable of distinguishing between ideal $Y^{3+}V^{3+}O_3$ and $Y^{3+}_{0.987}V^{3+}_{0.987}O_{2.961}$ containing both cation and oxygen vacancies. Resistivity measurements could give some information, but accurate resistivity measurements of insulating materials are difficult, and one needs dense ceramics for measurements and a standard sample for comparison. Accurate density measurements seem to be the only method to distinguishing between $YVO_3$ and $Y_{0.987}V_{0.987}O_{2.961}$.


dx.doi.org/10.1021/ic401042x | Inorg. Chem. 2013, 52, 8529−8539

During the high-pressure treatment of AP-$YVO_3$, the sample is slightly oxidized. The same process seems to occur during crystal growth by a floating-zone method at ambient pressure because the reported composition of single crystals was $YVO_{3.03(2)}$ and $YVO_{3.02}$.[6,12] The process corresponds to a transition from $YVO_3$ (or $Y_{0.987}V_{0.987}O_{2.961}$) to cation-deficient $Y_{0.987}V_{0.987}O_3$, and it should involve ion/vacancy migration through crystallites. Reaching the equilibrium of vacancy distribution requires time. HP-$YVO_3$ and HP-$YVO_3$(II) were very similar to each other (as discussed above; except for magnetic properties). They were annealed at high pressure during different time: a short period of 15 min for HP-$YVO_3$(II) and a long period of 130 min for HP-$YVO_3$. Therefore, at this point, we can suggest that quite different magnetic properties of HP-$YVO_3$ and HP-$YVO_3$(II) are originated from different annealing time and, as a result, from different distribution of ion vacancies (or defects, in general). HP-$YVO_{3.041}$ and single crystals of $YVO_{3+\delta}$ (which are slowly grown) could reach an equilibrium distribution of defects, and they demonstrate similar magnetic properties.

It is interesting to note that there was a plateau-like anomaly near 770 K in the weight increase on the TG curve of AP-$YVO_3$ and a corresponding anomaly on the DTA curve centered at 757 K (Figure S3, Supporting Information). The oxygen content near the plateau was about $YVO_{3.040}$ (at 765 K) and $YVO_{3.055}$ (at 780 K). That oxygen content was close to the oxygen content of HP-$YVO_{3.041}$ and HP-$YVO_{3.053}$(II). Therefore, the presence of the plateau might reflect the existence of thermodynamically stable partially oxidized phases of $YVO_{3+\delta}$.

We found that the MR effect appears in HP-$YVO_3$ only after cooling in moderate fields (and even small trapped fields) through $T_{N1}$. No MR effect was observed when HP-$YVO_3$ was cooled in a zero magnetic field through $T_{N1}$, and a field was applied below $T_{N1}$ (Figures 9b and 10a). We observed clear features of the EB effect in AP-$YVO_3$, HP-$YVO_3$(II), and HP-$YVO_3$ (Figure 11), and EB was tunable in HP-$YVO_3$. The tunable EB in HP-$YVO_3$ should be responsible for the MR effect.[25,30] Exchange bias is a property of a coupled AFM-FM system,[25] and the effect is due to magnetic interface interactions.[31,32] Therefore, we should first ask ourselves "what are the origin and mechanism of the (tunable) EB effect in $YVO_3$" instead of "what is the origin of the MR effect". This question is principally different from all previous works because it allows looking at the problem from a different viewpoint. The primary question can, in turn, be separated into several secondary questions.

The first question is: "what is the origin of an FM part in $YVO_3$?" It is probably the anomaly at $T_{FM}$, which is higher than $T_{N1}$. However, the origin of the anomaly at $T_{FM}$ is still a mystery to be solved. First, the possibility of a real magnetic impurity should not be ruled out even in "single-phase" and single-crystal materials. Second, the anomaly at $T_{FM}$ could be a surface phase transition. A surface transition was recently detected in another simple perovskite $BiFeO_3$ (in bulk form), and that surface transition could be seen in magnetic measurements.[33] It was argued that $BiFeO_3$ cannot be considered as a homogeneous material anymore because its skin layer is quite different from the bulk with its own structural and magnetic properties.[33] Third, explanations given in refs 3, 26, and 27 as "short-range order" and "local structural disorder on V atoms" could also be valid. Very detailed and careful studies are needed to determine the origin of the anomaly at $T_{FM}$; they are out of the scope of the present work because they will require different approaches and methods.

To illustrate the importance of the anomaly at $T_{FM}$ we performed the following experiments. HP-$YVO_3$ and AP-$YVO_3$ were cooled from 300 to 5 K in a negative field of −10 kOe, then a magnetic field of 100 Oe was applied at 5 K, and the susceptibility measurements were performed on heating from 5 to 300 K. In the case of AP-$YVO_3$, negative magnetization was observed from 5 to 135 K, that is, noticeably higher than $T_{N1}$ (see Figure S7 in the Supporting Information). This fact shows that some spins aligned by the negative field of −10 kOe remained in this direction under the opposite field of +100 Oe even in a paramagnetic region where bulk spins should follow the external field. Despite a large number of papers on properties of single crystals of $YVO_3$, there is no clear information whether single crystals of $YVO_3$ show magnetic anomalies at $T_{FM}$ or not. Anomalies at $T_{FM}$ in polycrystalline $YVO_3$ were well documented.[3,26]

The only anomaly at $T_{FM}$ cannot be responsible for the appearance of the tunable EB effect (and the MR effect) in HP-$YVO_3$ because AP-$YVO_3$, HP-$YVO_3$, and HP-$YVO_3$(II) showed similar anomalies at $T_{FM}$ (Figures 6−8). Therefore, the interaction of the FM part (in minority) with the AFM part (in majority) is crucial. This interaction leads to negative EB in AP-$YVO_3$ and HP-$YVO_3$(II) at all temperatures (and the absence of the MR effect, as a result), but to the positive EB in HP-$YVO_3$ between $T_{N2}$ and $T^*$. The nature of this interaction is also a mystery to be solved.

Another secondary question is: "what is the origin of interfaces in $YVO_3$?" There are interfaces between regions with defects (caused by the presence of vacancies and $V^{4+}$ ions) and ideal regions. There is interface between the surface layer and the bulk. Interfaces could form during low-temperature phase transformations and incomplete phase transitions. For example, phase separation and coexistence of two crystallographic phases down to 5 K was observed in $SmVO_3$, which shows MR.[34] Uncompensated spins could form near defects, surface, phase boundaries, and other inhomogeneities, and they could be differently pinned in AP-$YVO_3$, HP-$YVO_3$, and HP-$YVO_3$(II) considering their different defect chemistry, crystallinity, and particle size.

$YVO_3$ is an almost pure antiferromagnet below $T_{N2}$. At least, no spin canting was detected from neutron diffraction studies,[7,13] and we observed no anomalies on the $\chi''$ vs $T$ curves at $T_{N2}$ (Figure 5b). However, magnetization remained positive even at −10 kOe during the FC $M-H$ measurements (Figure 11 and Figures S16, S18, S20, and S27, Supporting Information) in this AFM material. This result can only be understood assuming that some spins aligned during the FC procedure remain in the same direction because they are tightly pinned and do not follow the external field.

Majority of perovskite materials with the MR effect crystallize in the $GdFeO_3$-type structure[35] with space group *Pnma* (with some exceptions, for example, HP-$BiFe_{1-x}Mn_xO_3$[21,36] and AP-$BiFe_{1-x}Mn_xO_3$[36]). Magnetic behavior of those perovskite materials with the MR effect can be described as follows. On cooling in moderate magnetic fields (the FCC mode), magnetization shows small jumps on crossing $T_N$ because of the appearance of a weak intrinsic ferromagnetic moment. On further cooling, the magnetization reaches maximum. The maximum can be rather sharp (e.g., in $LaVO_3$)[3,16,37,38] or very broad (e.g., $La_{0.15}Pr_{0.85}CrO_3$,[23] $La_{0.2}Ce_{0.8}CrO_3$,[24] $TmCrO_3$,[39] $NdVO_3$,[16] and $BiFe_{0.6}Mn_{0.4}O_3$).[21] After the maximum, the


dx.doi.org/10.1021/ic401042x | Inorg. Chem. 2013, 52, 8529−8539

magnetization gradually decreases and crosses the zero value at a certain compensation temperature ($T^*$). $T^*$ is usually field- and sample-dependent. The situation in $YVO_3$ (and, for example, in $TmCrO_3$)[39] is complicated because of the existence of $T_{N2}$, when the magnetic state established below $T_{N1}$ is changed, and the magnetization sharply returns to its normal positive value below $T_{N2}$. All materials, where detailed studies have been performed, show tunable EB.[14,17,21,23,24,37,39,40] There are few examples (e.g., $YVO_3$ and $BiFe_{0.6}Mn_{0.4}O_3$)[21] where ferromagnetic-like anomalies ($T_{FM}$) were detected above $T_N$, but the small number of examples could probably be caused by the fact that little attention has been paid. Perovskite materials with the MR and EB effects have different compositions at the *A* and *B* sites.[35] Taking $YVO_3$ as an example, the influence of magnetic rare-earth ions at the *A* site, the coupling between cations at the *A* and *B* sites, the existence of different competing magnetic interactions between different ions at the *B* site, and the nanosized nature of materials can be ruled out as the primary origin of the MR and EB effects in perovskites. We suggest that their similar behavior is caused by the existence of pinned uncompensated interfacial spins and weak intrinsic ferromagnetic moments, and pinned spins are originated from different inhomogeneities. In general, the origin of inhomogeneities can be quite different depending on the system. For example, clustering effects were suggested in $BiFe_{1-x}Mn_xO_3$[21] and observed experimentally by Mössbauer spectroscopy.[22] A skin layer was observed in $BiFeO_3$.[33] Dopant segregation[41] and phase separation sometimes take place.[25,34] Secondary phases were observed in bulk and thin films of $BiFeO_3$, and EB was associated with interfaces between the primary and secondary phases.[42,43] In $YVO_3$, vacancies and $V^{4+}$ ions are probably responsible for inhomogeneities.

## 5. CONCLUSION REMARKS

Our results provide significant contribution to understanding the mystery of the magnetization reversal effects in $YVO_3$ and allow looking at the problem from a different viewpoint. Tunable exchange bias should be responsible for magnetization reversal in $YVO_3$. We demonstrated that magnetization reversal is not an exclusive property of single crystals, but some polycrystalline samples of $YVO_3$ also exhibit magnetization reversal. By finding conditions under which no magnetization reversal occurs (upon crossing $T_{N2}$ and $T^*$ at moderate magnetic fields), we suggested that magnetization reversal is not an intrinsic property of $YVO_3$. By the intrinsic property, we mean a property caused by exchange interactions among homogeneous spins of $V^{3+}$ ions in bulk. We observed a drastic effect of trapped magnetic fields on the magnetization reversal effect, the memory effect (when a sample remembers how it was cooled through $T_{N1}$), remarkable exchange bias effects in polycrystalline $YVO_3$, and tunable exchange bias effect in HP-$YVO_3$. We suggested that "positive exchange bias", "defects", "interfaces", and "pinning" should be keywords for understanding $YVO_3$ and probably other perovskite materials exhibiting magnetization reversal in addition to or instead of "single-ion magnetic anisotropy" and "Dzyaloshinsky–Moriya interaction" keywords; and a general fundamental question should be: "what are the origin and mechanism of exchange bias in (seemingly) single-phase and homogeneous materials?"

## ■ ASSOCIATED CONTENT

### Supporting Information

Complete ref 33, more details in the experimental part and discussion, structural data, and details of magnetic properties of AP-$YVO_3$, HP-$YVO_3$, HP-$YVO_3$(II), and HP-$YVO_3$(b) (pellets, fixed powder, and free powder). This material is available free of charge via the Internet at http://pubs.acs.org.

## ■ AUTHOR INFORMATION

### Corresponding Author

*E-mail: alexei.belik@nims.go.jp.

### Notes

The authors declare no competing financial interest.

## ■ ACKNOWLEDGMENTS

This work was supported by World Premier International Research Center Initiative (WPI Initiative, MEXT, Japan), the Japan Society for the Promotion of Science (JSPS) through its "Funding Program for World-Leading Innovative R&D on Science and Technology (FIRST Program)", and the Grants-in-Aid for Scientific Research (22246083) from JSPS, Japan.

## ■ REFERENCES

(1) Zhou, J.-S.; Goodenough, J. B.; Yan, J.-Q.; Ren, Y. *Phys. Rev. Lett.* **2007**, *99*, 156401.
(2) Yan, J.-Q.; Zhou, J.-S.; Goodenough, J. B.; Ren, Y.; Cheng, J. G.; Chang, S.; Zarestky, J.; Garlea, O.; Llobet, A.; Zhou, H. D.; Sui, Y.; Su, W. H.; McQueeney, R. J. *Phys. Rev. Lett.* **2007**, *99*, 197201.
(3) Nguyen, H. C.; Goodenough, J. B. *Phys. Rev. B* **1995**, *52*, 324.
(4) Yan, J.-Q.; Zhou, J.-S.; Goodenough, J. B. *Phys. Rev. B* **2005**, *72*, 094412.
(5) Ren, Y.; Palstra, T. T. M.; Khomskii, D. I.; Pellegrin, E.; Nugroho, A. A.; Menovsky, A. A.; Sawatzky, G. A. *Nature* **1998**, *396*, 441.
(6) Ren, Y.; Palstra, T. T. M.; Khomskii, D. I.; Nugroho, A. A.; Menovsky, A. A.; Sawatzky, G. A. *Phys. Rev. B* **2000**, *62*, 6577.
(7) Ulrich, C.; Khaliullin, G.; Sirker, J.; Reehuis, M.; Ohl, M.; Miyasaka, S.; Tokura, Y.; Keimer, B. *Phys. Rev. Lett.* **2003**, *91*, 257202.
(8) Horsch, P.; Khaliullin, G.; Oles, A. M. *Phys. Rev. Lett.* **2003**, *91*, 257203.
(9) Blake, G. R.; Palstra, T. T. M.; Ren, Y.; Nugroho, A. A.; Menovsky, A. A. *Phys. Rev. Lett.* **2001**, *87*, 245501.
(10) Fang, Z.; Nagaosa, N. *Phys. Rev. Lett.* **2004**, *93*, 176404.
(11) Solovyev, I. V. *Phys. Rev. B* **2006**, *74*, 054412.
(12) Blake, G. R.; Palstra, T. T. M.; Ren, Y.; Nugroho, A. A.; Menovsky, A. A. *Phys. Rev. B* **2002**, *65*, 174112.
(13) Reehuis, M.; Ulrich, C.; Pattison, P.; Ouladdiaf, B.; Rheinstadter, M. C.; Ohl, M.; Regnault, L. P.; Miyasaka, M.; Tokura, Y.; Keimer, B. *Phys. Rev. B* **2006**, *73*, 094440.
(14) (a) Kimishima, Y.; Ichiyanagi, Y.; Shimizu, K.; Mizuno, T. *J. Magn. Magn. Mater.* **2000**, *210*, 244. (b) Kimishima, Y.; Nishida, S.; Mizuno, T.; Ichiyanagi, Y.; Uehara, M. *Solid State Commun.* **2002**, *122*, 519.
(15) Kimishima, Y.; Uehara, M.; Saitoh, T. *Solid State Commun.* **2005**, *133*, 559.
(16) Tung, L. D.; Lees, M. R.; Balakrishnan, G.; McK. Paul, D. *Phys. Rev. B* **2007**, *75*, 104404.
(17) Mao, J. H.; Sui, Y.; Zhang, X. Q.; Wang, X. J.; Su, Y. T.; Liu, Z. G.; Wang, Y.; Zhu, R. B.; Wang, Y.; Liu, W. F.; Liu, X. Y. *Solid State Commun.* **2011**, *151*, 1982.
(18) Mao, J. H.; Sui, Y.; Zhang, X. Q.; Su, Y. T.; Wang, X. J.; Liu, Z. G.; Wang, Y.; Zhu, R. B.; Wang, Y.; Liu, W. F.; Tang, J. K. *Appl. Phys. Lett.* **2011**, *98*, 192510.
(19) Dasari, N.; Mandal, P.; Sundaresan, A.; Vidhyadhiraja, N. S. *Europhys. Lett.* **2012**, *99*, 17008.

(20) Mandal, P.; Sundaresan, A.; Rao, C. N. R.; Iyo, A.; Shirage, P. M.; Tanaka, Y.; Simon, C.; Pralong, V.; Lebedev, O. I.; Caignaert, V.; Raveau, B. *Phys. Rev. B* **2010**, *82*, 100416.
(21) Belik, A. A. *Inorg. Chem.* **2013**, *52*, 2015.
(22) Delmonte, D.; Mezzadri, F.; Pernechele, C.; Calestani, G.; Spina, G.; Lantieri, M.; Solzi, M.; Cabassi, R.; Bolzoni, F.; Migliori, A.; Gilioli, E. arXiv:1302.7231 [cond-mat.mtrl-sci].
(23) Yoshii, K. *Appl. Phys. Lett.* **2011**, *99*, 142501.
(24) Manna, P. K.; Yusuf, S. M.; Shukla, R.; Tyagi, A. K. *Appl. Phys. Lett.* **2010**, *96*, 242508.
(25) (a) Nogues, J.; Schuller, I. K. *J. Magn. Magn. Mater.* **1999**, *192*, 203. (b) Berkowitz, A. E.; Takano, K. *J. Magn. Magn. Mater.* **1999**, *200*, 552.
(26) Corti, M.; Cintolesi, F.; Lascialfari, A.; Rigamonti, A.; Rossetti, G. *J. Appl. Phys.* **1997**, *81*, 5286.
(27) Massa, N. E.; Piamonteze, C.; Tolentino, H. C. N.; Alonso, J. A.; Martínez-Lope, M. J.; Casais, M. T. *Phys. Rev. B* **2004**, *69*, 054111.
(28) Izumi, F.; Ikeda, T. *Mater. Sci. Forum* **2000**, *321*−*324*, 198.
(29) Kumar, N.; Sundaresan, A. *Solid State Commun.* **2010**, *150*, 1162.
(30) Li, Z.-P.; Eisenmenger, J.; Miller, C. W.; Schuller, I. K. *Phys. Rev. Lett.* **2006**, *96*, 137201.
(31) Ohldag, H.; Scholl, A.; Nolting, F.; Arenholz, E.; Maat, S.; Young, A. T.; Carey, M.; Stöhr, J. *Phys. Rev. Lett.* **2007**, *91*, 017203.
(32) Wu, S. M.; Cybart, S. A.; Yi, D.; Parker, J. M.; Ramesh, R.; Dynes, R. C. *Phys. Rev. Lett.* **2013**, *110*, 067202.
(33) Jarrier, R.; et al. *Phys. Rev. B* **2012**, *85*, 184104.
(34) Sage, M. H.; Blake, G. R.; Nieuwenhuys, G. J.; Palstra, T. T. M. *Phys. Rev. Lett.* **2006**, *96*, 036401.
(35) Moure, C.; Pena, O. *J. Magn. Magn. Mater.* **2013**, *337*, 1.
(36) Belik, A. A.; Abakumov, A. M.; Tsirlin, A. A.; Hadermann, J.; Kim, J.; Van Tendeloo, G.; Takayama-Muromachi, E. *Chem. Mater.* **2011**, *23*, 4505.
(37) Mahajan, A. V.; Johnston, D. C.; Torgeson, D. R.; Borsa, F. *Phys. Rev. B* **1992**, *46*, 10966.
(38) Miyasaka, S.; Okimoto, Y.; Iwama, M.; Tokura, Y. *Phys. Rev. B* **2003**, *68*, 100406(R).
(39) Yoshii, K. *Mater. Res. Bull.* **2012**, *47*, 3243.
(40) Hong, F.; Cheng, Z. X.; Wang, J. L.; Wang, Z. L.; Dou, S. X. *Appl. Phys. Lett.* **2012**, *101*, 102411.
(41) Bernardo, M. S.; Jardiel, T.; Peiteado, M.; Mompean, F. J.; Garcia-Hernandez, M.; Garcia, M. A.; Villegas, M.; Caballero, A. C. *Chem. Mater.* **2013**, *25*, 1533.
(42) Sung, K. D.; Park, Y. A.; Seo, M. S.; Jo, Y.; Hur, N.; Jung, J. H. *J. Appl. Phys.* **2012**, *112*, 033915.
(43) Maity, T.; Goswami, S.; Bhattacharya, D.; Roy, S. *Phys. Rev. Lett.* **2013**, *110*, 107201.